Mid-Frequency Geoacoustic Inversion of Source Tow Data From the ASIAEX East China Sea Experiment

Chen-Fen Huang and William S. Hodgkiss
Marine Physical Laboratory
Scripps Institution of Oceanography
La Jolla, CA 92093-0238
Email: chenfen@mpl.ucsd.edu

***Abstract*— During the 2001 ASIAEX East China Sea experiment, source tow data were collected by a 16-element, 75-m aperture vertical line array in 105 m deep water. Continuous wave tonals at 95, 195, 295, 395, 805, 850, and 905 Hz were transmitted from a J-15 transducer at a nominal depth of 47 m. An environmental model in the study area initially was derived by matched-field geoacoustic inversion using the low frequency data (195, 295, and 395 Hz). The quality of the inversion was checked by source localization over an interval of time while the source range varied from 1 to 3.5 km. In this study, the mid-frequency data (805, 850, and 905 Hz) are incorporated into the inversion procedure. The results indicate that the bestfit model found using the lower frequency band can be extended one-octave higher in the application of MFP source localization despite higher sidelobe levels. The quality of the refined model again is confirmed by time-continuous, source localization using the higher frequency data over the same time interval.**

I. Introduction

Probing geoacoustic properties indirectly from acoustic sound fields in an oceanic environment is an important application of underwater sound. Based upon waveguide physics, acoustic sound fields interact with various components of the environment.

Here, matched-field (MF) inversion techniques are applied to estimate the environmental parameters during the 2001 ASIAEX East China Sea experiment. The basic principle of the MF inversion technique is to estimate the unknown parameters by minimizing an objective function that quantifies the mismatch between measured acoustic fields and simulated replica fields derived from an acoustic propagation model in a parameterized environment. The best estimates for the unknown parameters then correspond to the lowest mismatch. Since the dimension of the search space depends upon the number of unknown parameters which sometimes may be large, an efficient algorithm is needed to optimize the global search procedure. The genetic-algorithm-based software SAGA [1] is used in this analysis along with the normal-mode propagation model SNAP [2] for a range-independent environment.

Most experimental studies have reported successful geoacoustic inversion results using frequencies below 500 Hz [3]–[5]. An environmental model in this study area initially was derived by MF geoacoustic inversion using low frequency data (195, 295, and 395 Hz) [6]. The purpose of this paper is to incorporate higher frequency tonals (805, 850, and 905 Hz) into the geoacoustic inversion. The quality of the refined model is confirmed by time-continuous, source localization using the higher frequency data over a 30-min time interval.

II. ASIAEX 2001 East China Sea Experiment and Data Processing

The map of the region where the acoustic and oceanographic measurements were taken is shown in Fig. 1. On Julian Day (JD) 158 of 2001, acoustic energy was transmitted from the J-15 source towed near 47-m depth by R/V Melville with a speed of about 3 knots. The ship track is indicated by the thick line in the figure, on which the distances between the source and the receiver range from 0.5 to 6 km. A 16-element, 75-m aperture, autonomous recording vertical line array (VLA) was moored up from the seafloor where the water depth was

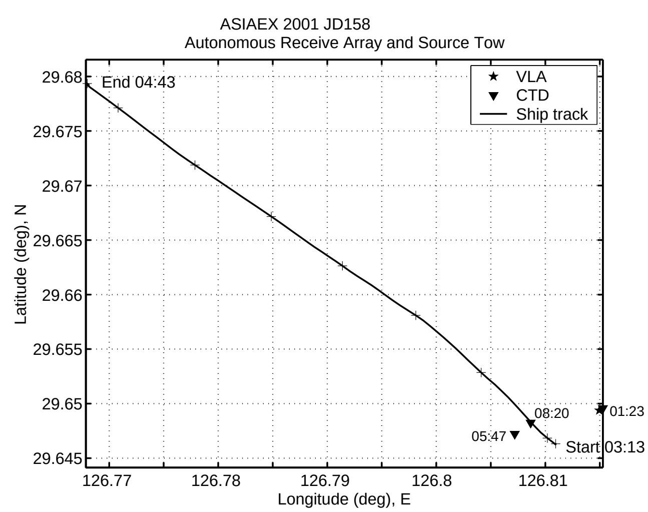

Fig. 1. Plan view of the ASIAEX 2001 East China Sea experiment. The thick line represents the ship track where the source energy was transmitted, and the plus signs mark 10-minute intervals starting from the acoustic measurement. The triangle signs represent the locations where the CTD measurements were taken. The star sign indicates the location of the vertical line array (VLA). All times are in Greenwich Mean Time (GMT).

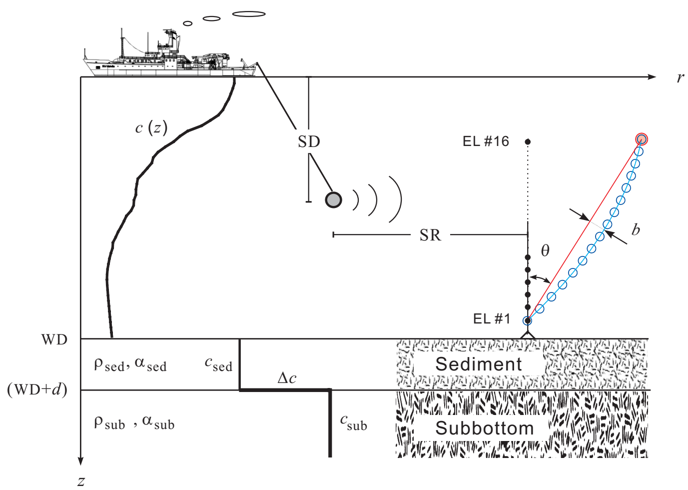

Fig. 2. Geoacoustic model and experimental configuration for the ASIAEX 2001 East China Sea experiment. Thick lines indicate schematically the sound speed distribution in the water and in the bottom. For the nomenclature, see Table I.

approximately 105 m. Continuous-wave (CW) tonals at 95, 195, 295, 395, 805, 850, and 905 Hz were transmitted and the sound field were recorded from 0313 to 0443 Greenwich Mean Time (GMT).

For current measurements, the current profile in the water column from 30 to 100 m was obtained by a ship-mounted ADCP system on board R/V Melville. During the acoustic transmissions, there existed a strong tidal current with magnitude greater than 0.5 m/s around the middle of the water column.

For sound speed measurements, three CTDs were taken on JD 158. Typical summer sound-speed profile characteristics were observed with significant fluctuations in the thermocline. Additional details of the experiment can be found in [6].

The entire 90-minute time series data were processed using 262,144-point FFTs with 50% overlap. With a sampling rate of 20470.8 samples/sec, the time duration of each FFT (snapshot) is 12.805 sec, and the interval between consecutive snapshots is 6.40 sec. The long length of the snapshot is to ensure high signal-to-noise ratio (SNR). The signal frequency at 95 Hz was discarded due to poor SNR.

The estimated normalized cross-spectral density matrix (CSDM), $\widehat{\mathbf{R}}$, for a signal frequency is given by

$$\widehat{\mathbf{R}} = \frac{\langle \mathbf{d}\mathbf{d}^{\dagger} \rangle}{\mathrm{Tr}\left[\langle \mathbf{d}\mathbf{d}^{\dagger} \rangle\right]}, \tag{1}$$

where $\mathbf{d}$ is the vector containing the measured complex pressures registered at the receivers, and $\langle\cdot\rangle$ and $\dagger$ denote, respectively, the average over several snapshots and the complex transpose operation. The covariance matrix is normalized by its trace. Under the assumption of statistical stationarity, each value of CSDM was estimated from 4 snapshots which span a time interval of 32 sec and cover about 48 m in source range.

III. Matched-Field Geoacoustic Inversion

The procedure and the required components for the MF geoacoustic inversion are summarized as follows.

A. Acoustic Propagation Model

For ranges greater than several water depths, the acoustic pressure field may be expressed as a finite sum of normal modes. A general bathymetric and geological survey has indicated that in the neighborhood of the experimental site the environment is nearly range-independent. Therefore, the acoustic pressure at a depth z and range r produced by a time-harmonic $e^{-i\omega t}$ point source at depth z_s in an environment with arbitrary sound speed distribution may be expressed as

$$p(r,z) = \frac{ie^{-i\pi/4}}{\rho(z_s)\sqrt{8\pi r}} \sum_{n=1}^{N} \Psi_n(z_s)\Psi_n(z)\frac{e^{ik_{rn}r}}{\sqrt{k_{rn}}} \tag{2}$$

where Ψ_n is the n-th normal mode corresponding to the horizontal wavenumber, k_{rn}. The calculations of the modeled acoustic pressure fields were performed by the SACLANTCEN Normal-mode Acoustic Propagation program (SNAP) [2].

B. Baseline model

The baseline model consists of an ocean layer overlying a sediment layer and a subbottom layer as shown schematically in Fig. 2. All layers were assumed to be range independent. The model parameters were divided into three subsets: geometrical, geoacoustic, and ocean sound speed parameters. The geometrical parameters include source range, source depth, water depth, and the array shape (array tilt and bow). The geoacoustic parameters include sediment compressional speed, density, attenuation and thickness, and subbottom compressional speed (subbottom density and attenuation are fixed at 2.4 g/cm^3 and 0.01 dB/λ, respectively). Note that the sound speeds in these two layers are related by the sound speed difference between the two layers. The ocean sound speed was modeled by a linear combination of empirical orthogonal functions (EOFs). An empirical orthogonal function (EOF) analysis at the experimental site shows that the first 3 EOFs contain about 90% of the energy. Therefore, the number of representative EOFs was set to three in the original low frequency inversion.

The total number of model parameters included in the low frequency inversion was 13. The parameter values can be found in [6] and are tabulated in Table I.

C. Objective Function

The objective function measures the discrepancy between the measured acoustic field and replica fields calculated for likely values of the unknown parameters. The data misfit objective function chosen here is based on the incoherent multifrequency Bartlett processor [7]. Under the assumption of no spatial coherence across frequencies, the misfit objective

TABLE I

INVERSION PARAMETERS AND THEIR ESTIMATED VALUES AT SR = 1.7 KM USING 195, 295, AND 395 HZ.

Parameter		SAGA$_{\text{best}}$	SAGA$_{\text{mean}}$ $\pm\ \sigma$
Geometrical			
Source range (m)	SR	1714	1714 ± 16
Source depth (m)	SD	48.3	48.4 ± 0.2
Water depth (m)	WD	105.4	105.4 ± 0.6
Array tilt (deg)	θ	-6.02	-6.02 ± 0.08
Bow of parabola (m)	b	1.3	1.3 ± 0.1
Geoacoustic			
Sed. Comp. speed (m/s)	c_{sed}	1585	1588 ± 7
Sed. attenuation (dB/λ)	α_{sed}	0.28	0.2 ± 0.1
Sed. density (g/cm^3)	ρ_{sed}	1.8	1.8 ± 0.2
Thickness (m)	d	10	10 ± 3
Increase comp. speed (m/s)	Δc	74	43 ± 24
Ocean sound speed			
EOF 1		6.3	6.1 ± 0.6
EOF 2		-2.2	-2.0 ± 0.6
EOF 3		-1.6	-1.7 ± 0.7

σ indicates one standard deviation from the mean.
The array tilt refers to the angle with respect to the vertical axis (negative in the direction away from the source). A 1° tilt corresponds to a displacement of approximately 1.3 m of the topmost array element from its nominal position.

function can be expressed as

$$\phi(\mathbf{m}) = \frac{1}{L}\sum_{l=1}^{L}\left[1 - \mathbf{e}_l^{\dagger}(\mathbf{m})\widehat{\mathbf{R}}_l\mathbf{e}_l(\mathbf{m})\right] \quad (3)$$

$$= 1 - \frac{1}{L}\sum_{l=1}^{L} P_{\text{BT},l}(\mathbf{m}) \quad (4)$$

where $\mathbf{e}(\mathbf{m})$ is the replica field generated for the vector of unknown parameters $\mathbf{m}$, normalized to have unit length, $\widehat{\mathbf{R}}$ is an estimated CSDM as given in (1), and L is the number of source frequencies. The misfit objective function can be re-written as a function of the Bartlett power as shown in (4), in which the second term is the arithmetic mean of Bartlett powers over the selected frequencies. By minimizing the misfit objective function, the most likely values of the environmental parameters can be found.

D. Model Parameter estimation

Based upon the environmental parameter estimates obtained from the low frequency tonal data, the environmental models are re-optimized by incorporating the higher frequency data into the inversion.

Even though most of energy is in the first 3 sound speed structure EOF shape functions, the EOF reconstruction for the measured sound speed CTD0123 and CTD0547 indicates that EOFs 4 and 5 have significant energy as given in Table II. (Figure 3 shows these two CTD profiles. The time interval of the acoustic transmissions are bracketed by these two CTDs.) Therefore, we include these 2 additional EOF coefficients in the higher frequency inversion.

TABLE II

THE EOF COEFFICIENTS FOR THE MEASURED SOUND-SPEED PROFILES ON JD 158.

Measured SSP	EOF 1	EOF 2	EOF 3	EOF 4	EOF 5	EOF 6
CTD0123	9.39	-0.63	-0.80	1.97	2.20	-0.27
CTD0547	6.77	-2.50	0.52	2.79	0.03	-0.28
CTD0820	11.95	-4.04	-2.73	1.45	0.21	0.68

EOF i denotes the i-th EOF coefficient.

The total number of model parameters included in the inversion is now 15. The values of the GA parameters used here are as follows: the population size was set to 64, reproduction size was 0.5, crossover probability was 0.8, mutation probability was 0.05, number of iterations was 2500, and the number of parallel populations was set to 45. Approximately 112,500 forward models were run.

IV. RESULTS AND DISCUSSION

Matched-field geoacoustic inversion using all 6 frequencies was carried out at the same source-receiver range (1.7 km) over the search space of 15 parameters. Table III tabulates the estimated parameter values. Compared with the inversion results obtained from the low frequency data (Table I), it can be seen that the estimates of the geoacoustic parameters do not change much. However, it is likely that the estimated water depth is deeper than the true depth. (the measured water depth is 105 m with a margin of error of plus or minus 1 m). The biased estimation of water depth might result from accommodating possible deviations of other environmental parameters (for yielding the best matched-field response).

Figure 3 shows the comparison of the estimated sound-speed profiles from the two inversions: the low frequency data (the circles connected by a solid line) and all 6 frequency data (the crosses connected by a solid line).

Range/depth ambiguity surfaces are computed for each source frequency using the low-frequency-derived bestfit model and these are shown in Fig. 4(a). The bottom panels show the results of incoherently averaging Bartlett ambiguity surfaces using only the low (left) and only the mid- (right) frequency tonals. The ambiguity surfaces are normalized so that the peak levels are 0 dB. We see that incoherently averaging Bartlett ambiguity surfaces for the low frequency data suppresses the ambiguous sidelobes efficiently. For the mid-frequency data, no significant improvement is observed due to the relatively close frequency spacing of the signals (*i.e.*, the structure of the sidelobes is similar across these frequencies). However, there is no ambiguity about the true source location. The results indicate that we can extend the bestfit model found using the lower frequency band to one-octave higher in the application of MFP source localization despite higher sidelobe levels.

TABLE III

PARAMETER ESTIMATES AT SR = 1.7 KM USING 195, 295, 395, 805, 850, AND 905 HZ.

Parameter		$\text{SAGA}_{\text{best}}$
SR	(m)	1760
SD	(m)	49
WD	(m)	106.6
Bow	(m)	1.4
θ	(deg)	−6.06
c_{sed}	(m/s)	1581
Δc	(m/s)	73
d	(m)	10
α_{sed}	(dB/λ)	0.37
ρ_{sed}	(g/cm^3)	1.7
EOF 1		6.3
EOF 2		−1.0
EOF 3		−0.3
EOF 4		0.1
EOF 5		1.1

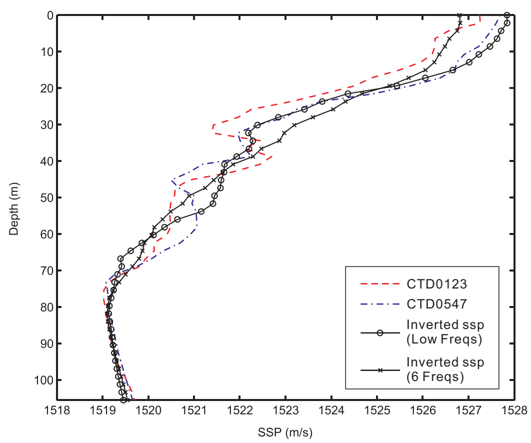

Fig. 3. Comparison of the estimated sound-speed profiles from two inversions: using the low frequency signals (the circles connected by a solid line) and using all 6 frequencies (the crosses connected by a solid line). The dashed and dashed-dotted lines indicate the measured sound speed profiles on JD158.

Next, ambiguity surfaces are computed for each source frequency using the all-6-frequency-derived bestfit model and these are shown in Fig. 4(b). As shown in the second column of Fig. 4(b), the sidelobe level is decreased significantly. The reason is that by incorporating the mid-frequencies into the geoacoustic inversion, mismatch in the environmental parameters has been minimized as far as the selected frequencies are concerned. As a result, not only is higher maximum Bartlett power achieved, but also sidelobe level is suppressed.

As a test, we use the low-frequency-derived bestfit model for source localization using only the mid-frequency signals over the time interval from 20 to 50 minutes. Figure 5 shows MF-derived source-receiver range (left panel) and source depth (right panel). The white line on each plot indicates where the environmental model is estimated. In the right panel, the plus signs indicate the source depths measured by the depth sensor. Based upon the GPS measurements, the data in this time interval cover the range from 1 to 3.5 km. We see that the maximum Bartlett power is low (less than −3 dB) at each range and there is some source position ambiguity.

Figure 6 demonstrates the performance of the all-6-frequency-derived bestfit model in source localization over the same time interval. Relatively high maximum Bartlett power at each range is achieved and the resulting source position is consistent with the experimental configuration up to 45 minutes.

V. CONCLUSION

This paper has discussed geoacoustic inversion results based upon source tow data obtained during the ASIAEX 2001 East China Sea experiment. The source tow data recorded on a VLA were used to estimate the geoacoustic properties of the seafloor. The waveguide was assumed to be range-independent and the seafloor was modeled as a homogeneous sediment layer overlying a semi-infinite subbottom.

Matched-field geoacoustic inversions using 195, 295, 395, 805, 850, and 905 Hz were carried out by a genetic-algorithm-based optimization approach. The inversion was performed with the set of data obtained at range of SR = 1.7 km. The quality of the inverted model was confirmed by time-continuous, source localization using the mid-frequency data over a 30-min time interval.

ACKNOWLEDGMENTS

This work was supported by the Office of Naval Research, Grant Nos. N00014-01-1-0096 and N00014-01-1-0171.

REFERENCES

[1] P. Gerstoft, *SAGA Users guide 4.0, an inversion software package*, An updated version of "SAGA Users guide 2.0, an inversion software package," SACLANT Undersea Research Centre, SM–333, La Spezia, Italy, 1997.

[2] F. B. Jensen and M. C. Ferla, *SNAP: the SACLANTCEN normal-mode acoustic propagation model*, SACLANT Undersea Research Centre, SM–121, La Spezia, Italy, 1979.

[3] P. Gerstoft and D. F. Gingras, "Parameter estimation using multifrequency range-dependent acoustic data in shallow water," *J. Acoust. Soc. Am.*, vol. 99, pp. 2839–2850, 1996.

[4] J. P. Hermand and P. Gerstoft, "Inversion of broadband multi-tone acoustic data from the YELLOW SHARK summer experiment," *IEEE J. Oceanic Eng.*, vol. 21, pp. 324–346, 1996.

[5] M. Siderius, M. Snellen, D. Simons, and R. Onken, "An environmental assessment in the Strait of Sicily: measurement and analysis techniques for determining bottom and oceanographic properties," *IEEE J. Oceanic Eng.*, vol. 25, pp. 364–386, 2000.

[6] C.-F. Huang and W. S. Hodgkiss, "Matched field geoacoustic inversion of low frequency source tow data from the ASIAEX East China Sea experiment," *IEEE J. Oceanic Eng.* (submitted, 2003).

[7] C. F. Mecklenbräuker and P. Gerstoft, "Objective functions for ocean acoustic inversion derived by likelihood methods," *J. Comp. Acoust.*, vol. 8, pp. 259–270, 2000.

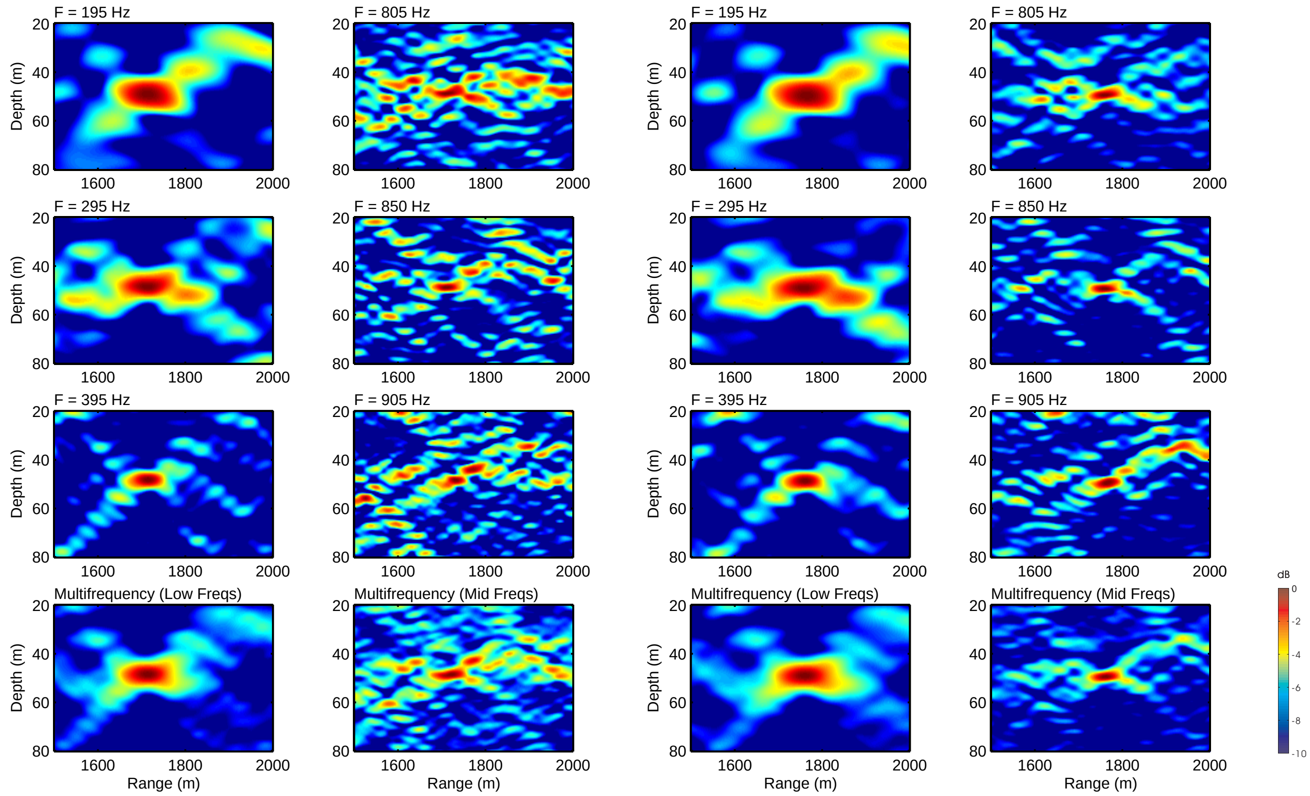

(a) Low-frequency-derived bestfit model

(b) All-6-frequency-derived bestfit model

Fig. 4. Range/depth ambiguity surfaces at SR $= 1.7$ km for each source frequency and the multifrequency average. (a) The replica pressure field is computed using the bestfit model derived from the low frequency signals (Table I). (b) The replica pressure field is computed using the bestfit model derived from all 6 frequencies (Table III). The estimated source position (SR and SD) and the Bartlett power obtained using the mid-frequency data are as follows: (a) (SR, SD) = (1722 m, 48.5 m) with Bartlett power = 0.415 and (b) (SR, SD) = (1761 m, 49.5 m) with Bartlett power = 0.626. On each ambiguity surface, the Bartlett power is normalized so that the peak level is 0 dB.

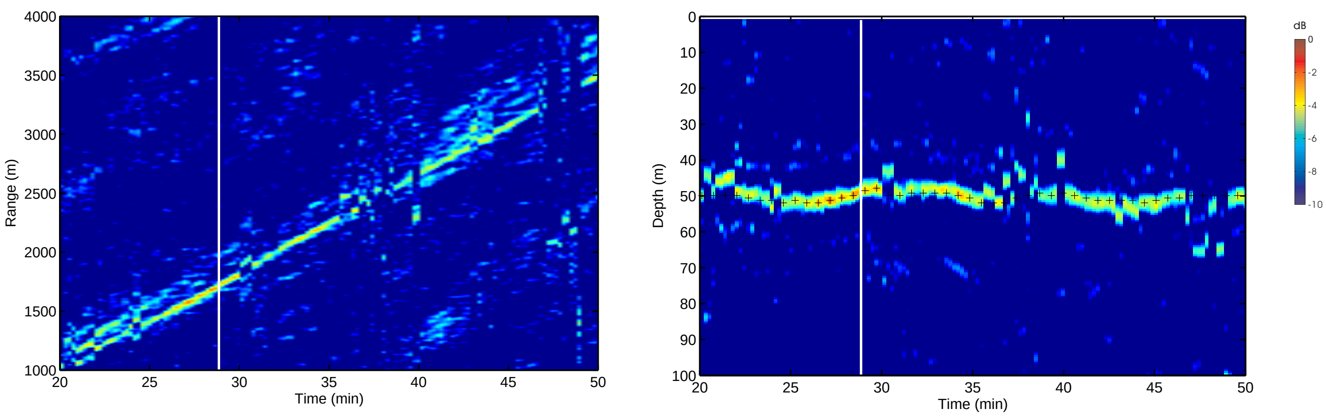

Fig. 5. MF-derived source-receiver range (left panel) and source depth (right panel) over the time interval from 20 to 50 min. The replica pressure field is computed using the low-frequency-derived bestfit model. The white line on each plot indicates where the environmental model is estimated. The plus signs (right panel) indicate the true measured source depths. Here, the Bartlett ambiguity surfaces have not been normalized at each range.

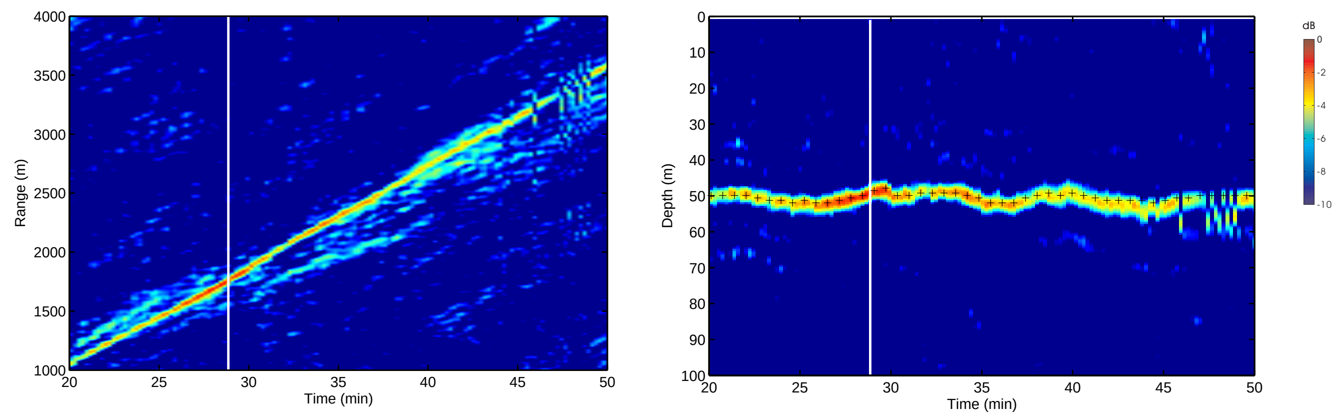

Fig. 6. MF-derived source-receiver range (left panel) and source depth (right panel) over the same time interval as in Fig. 5. The replica pressure field is computed using the bestfit model derived from all 6 frequencies. The white line on each plot indicates where the environmental model is estimated. The plus signs (right panel) indicate the true measured source depths.